AIChE

Modeling of Asphaltene Deposition in a Production Tubing

D. Eskin, J. Ratulowski, K. Akbarzadeh, and S. Andersen
Schlumberger DBR Technology Center, Edmonton, AB T6N 1M9, Canada

DOI 10.1002/aic.12800
Published online December 14, 2011 in Wiley Online Library (wileyonlinelibrary.com).

Asphaltene deposition phenomena are investigated both theoretically and experimentally. A Couette device, where the inner cylinder rotates and particles deposit on the outer wall, is used for deposition laboratory studies. A deposition modeling approach, recently proposed by the authors is improved. Empirical parameters of the model are obtained from Couette device experiments. The deposition mechanism peculiarities are explained based on an analogy between the deposition and water in oil emulsion stabilization by asphaltenes, and on an analysis of interaction of asphaltene molecules. The model performance is illustrated by modeling oil production, accompanied with asphaltene deposition, from a cylindrical reservoir through vertical tubing. The computations, performed for a reservoir depleting over time, demonstrate a good qualitative agreement with the field data reported in literature. © 2011 American Institute of Chemical Engineers *AIChE J,* 58: 2936–2948, 2012

Keywords: asphaltenes, aggregates, Couette device, deposition, pipe, turbulence

Introduction

Asphaltenes are complex molecular entities, which together with resins, aromatic hydrocarbons, and saturates compose crude oil. Asphaltene particles can precipitate from oil due to depressurization below the so-called asphaltene precipitation on-set pressure (AOP). Oil transport pipelines usually operate in a turbulent regime. The pressure gradually drops along a pipe, asphaltene particles precipitate, grow due to agglomeration with each other, and partially deposit on the pipeline walls. Modeling of asphaltene deposition in oil transport pipelines is required for more accurate forecasting of petroleum production problems caused by asphaltenes. The asphaltene deposit layer reduces pipe cross section that may lead to significant flow rate reduction and increased pressure drop. The deposit may eventually totally plug a pipeline.

We would like to mention two known articles containing field data on asphaltene deposition. The first is on deposition in oil well tubing's in Hassi Messaoud field by Haskett and Tartera.[1] A large number (322) of deposit layer profiles in vertical production tubing of 4.5 in. (1 in. = 25.4 mm) dia. in different wells and at different production rates were measured and analyzed. In some cases, the maximum deposit layer thickness reached $^2/_3$ of the tubing radius. It was found out that the maximum deposit thickness is usually obtained at that tubing cross section where the bubble point pressure is reached. The second notable article is dedicated to asphaltene deposition studies in West Kuwait by Alkafeef et al.[2] In that work, the asphaltene deposition hazard was clearly demonstrated. Monitoring the deposit layer thickness showed that in relatively small dia. (2.5 in.) tubing, the deposit thickness reached about $^1/_3$ of the tubing radius causing a significant increase in friction losses.

We can refer here to only a few articles on modeling the asphaltene deposition in pipelines. The first one was authored by Ramirez-Jaramillo et al.[3] These authors employed a hypothesis that the asphaltenes are transported to the wall due to molecular diffusion. They also assumed that the particle concentration gradient is caused by the temperature gradient at the wall. This modeling approach, borrowed from the well-developed theory of wax deposition (e.g., Burger et al.[4]) was not supported by our laboratory data. Our experiments on asphaltene deposition in a Couette device showed that there is no pronounced effect of the temperature gradient at the wall on the asphaltene deposition rate (Akbarzadeh et al.[5]). The second work was accomplished by Soulgani et al.[6] These researches fitted the asphaltene deposition rate by a simple correlation assuming that the deposition on the tubing surface is controlled by the chemical reaction mechanism. The known Arrhenius exponential term was employed as a basis for that correlation. No solid proofs supporting the suggested deposition mechanism was provided. The recent article of Vargas et al.[7] is more advanced in comparison with the predecessors. It includes the submodels describing the particle precipitation, agglomeration, transport and deposition on the wall. The aggregation and the deposition phenomena are modeled using pseudo-first-order reactions. The particle transport is described by the convection-diffusion equation. The diffusivity of asphaltene particles in a fluid flow was assumed to be constant and approximately equal to the measured diffusivity of asphaltenes in toluene. According to the model only small aggregates can stick to the wall surface and form a deposit. The model contains several parameters, needed to be identified from experiments. The authors demonstrated that their model accurately describes the asphaltene deposition in capillary tubes.

Correspondence concerning this article should be addressed to D. Eskin at deskin@slb.com.

Eskin et al.[8] developed a model of asphaltene deposition that is significantly different from the others. According to this model, the deposition occurs as follows. Asphaltene particles precipitate and then grow in a flow due to agglomeration with each other. It was assumed that the particle concentration is uniform over a pipe cross section and particles are transported to the wall, being involved in random fluctuations caused by both the Brownian motion and turbulence, and by turbophoresis. According to the introduced concept of the critical particle size, only particles of sizes smaller than the critical one can deposit on the wall. Only small percentage of particles touching the wall sticks to its surface. This percentage is determined by the particle-wall sticking probability that is also an empirical parameter of the model. A laboratory Couette device was employed for experimental identification of the model parameters. Tuning the model by the experimental data revealed very small critical particle sizes (30 and 72 nm for different oils), and very low (10^{-5}–10^{-6}) particle-wall sticking efficiencies (probabilities). Although the developed deposition model allowed matching the calculations results to the experimental data, physical causes of the extremely low values of the mentioned model parameters were not plausibly explained. A model performance was illustrated by computational examples of deposition in a laboratory Couette device and pipelines. Although deposit layer profiles, computed by Eskin et al.[8] were to some extent similar to those observed in the field,[1,2] an accuracy of the deposit thickness calculations was neither estimated nor discussed. An equation used for calculation of the deposit layer profile in a pipe was oversimplified because it was derived for an infinitely thin layer. An applicability of this equation to a thick layer was not proven. An effect of the reservoir characteristic on the deposition was not considered as well.

This work is an extensive development and improvement of the asphaltene deposition theory, earlier released by Eskin et al.[8] In this research, we will (1) simplify the model of particle growth, (2) introduce a more accurate model of particle transport to the wall, (3) present justification of the extremely low values of the critical particle size and the particle-wall sticking probability, (4) formulate an accurate algorithm of calculating the deposit layer thickness in a vertical pipe, producing from a simple cylindrical reservoir under steady-state conditions, and (5) account for an effect of the bottom-hole pressure reduction, caused by reservoir depletion, on the deposit layer profile. For enhancing the model credibility, a number of computational examples illustrating the deposition process, will be presented.

Simulation of the Asphaltene Deposition in a Pipe by Couette Device Experiments

Experimental equipment and procedures

A wide-gap Couette device (Figure 1) was employed for our experiments. The inner cylinder of the radius $r_0 = 14$ mm rotates and particles deposit on the outer immobile wall of the radius $R = 28$ mm. The volume of fluid needed for running our laboratory Couette device is relatively small (150cc, 1cc = 1 cm^3), which is convenient for testing numerous fluid samples.

In our laboratory we employ the Couette device based system operating in batch and flow-through regimes, respectively. In the case of the batch regime a Couette device is initially filled with a hydrocarbon fluid at a pressure well above the detected asphaltene onset pressure (AOP) at the given temperature. Then, the pressure is abruptly (during several minutes) reduced to a value slightly higher than the bubble-point pressure, and near where the maximum amount of precipitated asphaltene particles is expected. After that the Couette device is run with a certain rotation speed during a given time. At the end of the test, the oil inside the device is drained at the test pressure and the generated deposit that formed on the device wall is recovered with dichloromethane and then the asphaltene mass measured.

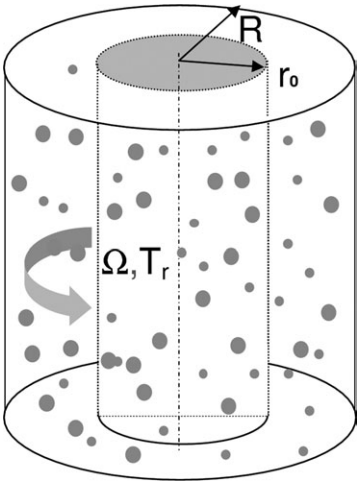

Figure 1. Couette device diagram.

A flow-through system is used to avoid the depletion effect on the deposition process. In this system, a continuous flow of a fresh fluid passes through the Couette device. A hydrocarbon fluid is initially placed in a one-liter storage bottle at high (reservoir) pressure. The sample bottle is connected to the Couette device inlet by a tube. The Couette device outlet is connected to a collecting cylinder. A back-pressure regulator and two automatic pumps are used to maintain the pressure of the sample storage bottle above the AOP pressure, while the pressure at the Couette device inlet is reduced to a value slightly higher than the BP pressure, and the pressure in the collecting cylinder is maintained close to the pressure in the Couette device. The flow-through rate is low, therefore, the mean fluid residence time in the Couette device is long enough to treat this device as an ideal mixer.

The flow-through system provides valuable information about the deposition process because the deposit amount collected can be much higher than that in the batch system. This is because during the constant influx of a fresh fluid no or minimal depletion occurs in the flow-through system.

Proper application of a Couette device for simulation of asphaltene deposition in a pipeline

To confidently employ a Couette device for deposition studies it was important to show that the deposition conditions in a pipeline can be simulated in a Couette device. One of the major requirements of deposition similarity in a Couette device and a pipeline is the same conditions of particle transport to the wall.

A flow pattern in both a pipeline and a Couette device can be considered as composed of a boundary layer flow and a core flow. Asphaltene particles are assumed to be well dispersed in a turbulent core flow. This is explained as follows. The density of asphaltene particles (aggregates) is usually

evaluated as $\rho_s = 1{,}200$ kg/m^3 while the fluid density is usually in the range of $\rho_f = 700$–1000 kg/m^3, i.e., the particle-fluid density difference is relatively small. The experimental observations show that sizes of absolute majority of asphaltene particles (aggregates) in a developed turbulent Couette flow do not exceed tens of micrometers (e.g., Rahmani et al.[9]). Therefore, the particle relaxation times are small enough to assume that those particles nearly follow fluid in both directed and fluctuation motions. Both the flow velocity and turbulence intensity rapidly change only within the boundary layer; therefore, the particle transport to the wall is mainly determined by the structure of this layer. It is easy to show (e.g., Bird et al.[10]) that the hydrodynamic similarity of two near-wall flows is obtained if the shear stress at the wall and the wall temperature, determining the fluid viscosity are the same.

The shear stress at the pipe wall is calculated as (e.g., Bird et al.[10])

$$\tau_w = \frac{1}{8} \cdot \rho_f f U^2 \tag{1}$$

where f is the Fanning friction factor that is a function of the pipe Reynolds number and the wall surface roughness, U is the superficial flow velocity, and ρ_f is the fluid density.

The maximum roughness of the transport pipe walls is usually below 50 μm. At the initial stage of the deposition process the cavities between asperities forming surface roughness are filled with deposit material; i.e., after a relatively short time the pipe surface is covered with a deposit. Therefore, despite the formed deposit thickness significantly varies along a pipe, the layer surface remains hydraulically smooth. Thus, for calculation of the Fanning friction factor the Blausius correlation (e.g., Bird et al.[10]) for a smooth pipe can be employed

$$f = \frac{0.316}{Re^{0.25}} \tag{2}$$

where $Re = UD/v_f$ is the pipe Reynolds number, D is the pipe diameter, and v_f is the fluid kinematic viscosity.

If the shear stress on the pipe wall is known, then the rotation speed of the Couette device rotor needed to provide the same shear stress on the outer wall of this device, can be calculated by an analytical equation relating the nondimensional torque G applied to the Couette device rotor and the Reynolds number Re_c (Eskin[11])

$$\frac{1.103\eta}{(1+\eta^2)(1-\eta)} \frac{Re_c}{\sqrt{G}} = \ln\sqrt{G} + \frac{2\eta}{1+\eta^2} - \ln\left(\frac{1+\eta}{1-\eta}\right) + 0.406 \quad \text{at} \quad Re_c \geq 1300 \tag{3}$$

where $G = T_r/(\rho_f v_f^2 L)$ is the dimensionless torque, L is the Couette device height; $\eta = r_0/R$ is the Couette device radius ratio; $Re_c = \omega r_0(R\text{-}r_0)/v_f$ is the Couette device Reynolds number; $T_r = \tau_w 2\pi R^2 L$ is the torque; ω the inner cylinder angular velocity.

Equation 3 is in a good agreement with the experimental data. In contrast to the other $G(Re_c)$ relations known from the literature (e.g., Lathrop et al.[12]) Eq. 3 does not contain any empirical parameters and is not limited to a single radius ratio η.

The restriction of the applicability of Eq. 3 to flows at relatively high-turbulence numbers ($Re_c > 13{,}000$) is caused by pronounced Taylor vortexes, strongly affecting mean flow field in a Couette device at lower Reynolds numbers. Thus, the flow dynamic analysis presented later is accurate only for the Reynolds numbers exceeding this threshold.

To evaluate an effect of the centrifugal force on particle dynamics in a Couette device a model for calculating the particle concentration distribution along the Couette device radius was developed (Eskin et al.[8]). The solution procedure was reduced to solving the advection-diffusion equation for particles moving in a rotating turbulent flow. Calculations were performed for our laboratory Couette device. It was clearly demonstrated (Eskin et al.[8]) that even at the relatively high-rotation speed of the inner cylinder (2950 rpm), the particle centrifugal stratification is small and can be ignored for asphaltene particles of sizes $d_s > 10$ μm. Because, as it will be shown later, only small submicron particles contribute into the deposition, the Couette device can be confidently employed for asphaltene deposition studies.

Deposition Model

Let us briefly describe the Couette device experiment, which was critical for understanding the deposition mechanism (Eskin et al.[8]). The Couette device, charged with certain oil, was run for 4 h at the flow-through fluid rate of 3 cm^3/min. After that, the deposit mass was determined and the deposition rate calculated. The deposited material was disposed. After that the fluid sample collected in the collecting cylinder was conditioned at reservoir pressure and temperature for 5 days to make sure that previously precipitated asphaltenes dissolved back into a fluid. The sample storage bottle was then filled with this conditioned fluid and the flow-through deposition experiment was repeated under the same conditions. The experiments showed that the measured deposition rate in the second experiment (15.6 g/m^2/day) was almost identical (even higher) to that in the first experiment (13.9 g/m^2/day).

Thus, the experiments demonstrated that removal of particles, deposited in the first experiment from the system, did not reduce the amount of particles, which are able to deposit that was shown by the second experiment. The hypothesis was that particles, able to deposit, are not stickier than other particles and the fluid depletion is not associated with disappearance of stickier particles from a fluid because of their deposition on the wall or agglomeration with other particles. We assumed that reduction of amount of particles, able to deposit, in time is caused by the particle growth due to agglomeration. Our primary guess was that the relatively large agglomerates, formed in a fluid, cannot deposit because they are removed from the wall by the viscous drag force. Based on this idea we introduced a concept of the critical particle size. Particles of sizes, larger than the critical one, cannot deposit under given flow conditions. As soon as all particles reach this size, the deposition completely stops indicating that a fluid is depleted of particles able to deposit.

We roughly evaluated the critical particle size based on the force balance applied to a particle attached to the wall (see Eskin et al.[8]). On the one hand, the particle is attracted to the wall by the Van der Waals force. On the other hand, the particle can be displaced from its position on the wall by the drag force and then immediately removed from the wall with a flow. Therefore, the critical particle size was evaluated on the basis of balance between the Van der Waals and the drag forces. The Van der Waals force was estimated by using the Fotland and Askvik's[13] data for the Hamaker constant for asphaltenes. The calculations showed how the

critical size decreases with an increase in the fluid viscosity and/or the mean flow velocity in a pipe: for the wide ranges of the fluid viscosity and the flow velocity the critical size varied from 2 to 35 μm. However, the further investigations by the developed deposition model[8] demonstrated that the critical size is significantly smaller (in the submicron range). The cause of such a small size value will be explained later in detail (see "Explanation of the deposition characteristics obtained by the developed model using analysis of asphaltene particle interactions with each other").

Particle-size distribution evolution modeling

The population balance approach was employed for modeling evolution of the particle-size distribution in Couette device over time. The Hounslow's version of this approach was used (e.g., Flesch et al.[14]). In this case a continuous size distribution is represented as a set of **im** discrete fractions. The volume of the i-th fraction is twice larger than that of the i-1 fraction. The set of equations describing the size distribution evolution in a batch Couette system is

$$\frac{dN_i}{dt} = N_{i-1}\sum_{j=1}^{i-2} 2^{j-i+1}\alpha_{i-1,j}\beta_{i-1,j}N_j + \frac{1}{2}\alpha_{i-1,i-1}\beta_{i-1,i-1}N_{i-1}^2 - N_i\sum_{j=1}^{i-1} 2^{j-i}\alpha_{i,j}\beta_{i,j}N_j - N_i\sum_{j=i}^{im-1}\alpha_{i,j}\beta_{i,j}N_j - S_iN_i + \sum_{j=i+1}^{im}\Gamma_{i,j}S_jN_j \qquad i,j = 1...im \tag{4}$$

where N_i is the concentration of particles of the i-th size fraction by number, $\beta_{i,j}$ is the collision frequency function of a particle of the i-th size fraction interacting with particles of the j-th size fraction, $\alpha_{i,j}$ is the collision efficiency of a particle of the i-th size fraction with that of the j-th size fraction, S_i is the fragmentation rate of the i-th size particle, and $\Gamma_{i,j}$ is the breakage distribution function indicating how many particles of the i-th size fraction are produced at breakage of a particle of the j-th size fraction.

The agglomerates can be treated as fractal objects with the fractal dimension D_f. According to the experiments of Rastegari et al.[15] the fractal dimension of asphaltene particles is about $D_f = 1.5$–1.8.

For calculating the collision frequency function, we employed the known model, described, for example, by Flesch et al.[14] According to this approach, the collision frequency function is calculated as superposition of the corresponding functions due to the particle Brownian motion and the turbulence fluctuations. This approach was recently employed by Eskin et al.[8] for modeling-size distribution of asphaltene particles. However, our latest numerical studies showed that in a system composed of agglomerating asphaltene particles, the concentration of submicron particles by number is overwhelmingly higher than that of larger particles. Therefore, the turbulent agglomeration mechanism can be confidently neglected and we can assume that the particle agglomeration is governed only by the Brownian motion characterized by the following collision frequency function

$$\beta_{i,j} = \frac{2}{3}\frac{k_B T}{\mu_f}\frac{(d_i + d_j)^2}{d_i d_j} \tag{5}$$

where $k_B = 1.3806504\cdot10^{-23}$ J/K is the Boltzmann constant.

Note that the particle size is evaluated by assuming that the shape factor of the real particle is the same as that of spherical particles $d_i = \left(\frac{6}{\pi}v_i\right)^{\frac{1}{D_f}}$.

The breakage term in the population balance equation, taken into account in the article of Eskin et al.[8] can also be neglected because submicron particles cannot be fragmented in a turbulent flow, characterized by the inner turbulence scale of the order of tens of micrometers (see, e.g., Levich[16]).

The most difficult problem of asphaltene population balance modeling is evaluation of the particle–particle collision efficiency $\alpha_{i,j}$. Because of not sufficient understanding of mechanism of the particle–particle interactions, it was assumed (Eskin et al.[8]) that the particle–particle collision efficiency α, in the model is a constant and does not depend on the particle size. The value of this constant is identified indirectly by fitting model results to experimental data.

An initial condition for population balance computations is the concentration of primary (precipitated particles) by number that is easily calculated if both the mass concentration of primary particles and the primary particle size are known. The mass concentration of primary particles can be determined either experimentally by measuring the mass of asphaltene particles, precipitated after pressure reduction within a given pressure range, or calculated by an asphaltene precipitation model (see, e.g., Du and Zhang[17]). A primary size of a precipitated particle is one of the most important parameters of the model.

According to the Betancourt's et al.[18] investigations, the asphaltene nanoaggregates, stable in a crude oil at the pressure earlier the AOP pressure, are characterized by the size of $\sim$1.6 nm that we employ as the primary particle size for our calculations. At the pressure reduction below the AOP pressure, the hydrocarbon system becomes thermodynamically unstable and the asphaltene nanoaggregates start growing (precipitate) due to the Brownian agglomeration.

The formulated population balance model is conventional and solution of the set of ordinary differential equations is straightforward. The important problem is obtaining experimental data needed to identify the particle–particle collision efficiency. It is impossible to measure particle-size distribution in the submicron size range. Eskin et al.[8] identified the particle–particle collision efficiency from the Couette device experimental data, which were the maximum particle sizes measured for different device run times by high-pressure microscope (HPM). The particle–particle collision efficiency, identified from those data, was around $\sim10^{-5}$.

To enhance credibility of such a low estimation of the particle–particle collision efficiency, we would like to shortly describe the results recently obtained by Maqbool et al.[19] Those authors modeled agglomeration of asphatenes precipitated from a crude oil due to destabilization by solvent. An experiment was performed in a stirring tank. By using microscope the investigators were able to roughly evaluate the size distribution of particles, size of which exceeded 0.5 μm. The population balance model was employed at accounting for only Brownian agglomeration mechanism. It was also assumed that the particles are spheres and the primary particle size is 2.5 nm. Maqbool et al.[19] were able to fit the computed results to the experimental data assuming an extremely low particle–particle sticking efficiency (of the order of magnitude of 10^{-6}).

Identification of very low particle–particle collision efficiency was an important result of those modeling efforts. An

existence of a very strong steric effect, preventing asphaltene particle agglomeration, was revealed. Because the major interest of our current work is the deposition of particles on the previously formed particle layer we can conclude that the probability of particle sticking to the asphaltene coated wall should be of the same order of magnitude as the particle–particle collision efficiency.

Let us now describe transport of particles of the given size distribution to the wall.

A model of particle transport to the wall

We assume that chaotically moving particles reach the wall being transported by Brownian motion and turbulence. The turbophoresis is neglected because our estimations showed that asphaltene particles, which can be effectively transported by this mechanism, have to be relatively large (roughly >50 μm); i.e., much larger than the critical particle size.

Eskin et al.[8] assumed that the particle concentration gradient at the wall of either a pipe or Couette device is zero. However, although the small particles are well dispersed over a flow domain by turbulence and the particle-wall sticking probability is very small, the concentration gradient in the wall vicinity is not obviously close to zero. This doubt is caused by the very low diffusivity of small particles in the wall vicinity and should be clarified.

Let us formulate the transport equations for particles of a single-size fraction. For the sake of simplicity, we will omit the subscript indicating a size fraction number.

The particle transport equation in a dimensionless form in this case is formulated as the expression for the dimensionless deposition velocity (e.g., Guha[20])

$$V_{dep}^{+} = -\left(D_t^{+}(y^{+}) + D_B^{+}\left(r_s^{+}\right)\right)\frac{dc^{+}}{dy^{+}} \tag{6}$$

where $D_B^{+} = D_B/\nu_f$ is the dimensionless Brownian diffusivity, $D_B = k_B T/3\pi\mu_f d_s$ is the Brownian diffusivity, $D_t^{+} = D_t/\nu_f$ is the dimensionless turbulent diffusivity, $c^{+} = c/c_0$ is the dimensionless solids concentration, c_0 is the mean solids concentration in a fluid system, $V_{dep}^{+} = J/u_*$ is the dimensionless deposition velocity, J is the volume particle flux per unit wall area, $y^{+} = y/\delta^{+}$ is the dimensionless y coordinate, $r_s^{+} = r_s/\delta^{+}$ is the dimensionless particle radius, and $\delta^{+} = \nu_f/u_*$ is the wall layer thickness.

In Eq. 6 we assumed that the particle turbulent diffusivity is equal to the fluid turbulent diffusivity because the transported particles are very small.

Let us formulate the boundary condition describing particle-wall interactions. The particle touches the wall if its center approaches the surface at the distance equal to the particle radius r_s. The particle concentration at this distance is $c(r_s)$. A particle located at this distance fluctuates due to both the Brownian and the turbulent fluctuation motions. However, the turbulence at the distance r_s for submicron particles is very small and can be neglected. Therefore, the dimensionless particle deposition velocity is expressed through the Brownian fluctuation velocity as

$$V_{dep}^{+} = \frac{1}{2}\gamma c^{+}\left(r_s^{+}\right)\upsilon_B^{+}\left(r_s^{+}\right) \tag{7}$$

where $\upsilon_B^{+}(r_s^{+})$ is normal to the wall component of the most probable particle fluctuation velocity in the Brownian motion at the moment of touching the wall, γ is the particle-wall sticking probability.

The multiplier $\frac{1}{2}$ in Eq. 7 indicates that at a certain time moment only a half of particles having the concentration $c^{+}(r_s^{+})$ moves toward the wall.

The normal to the wall component of the particle fluctuation velocity due to the Brownian motion is calculated as[8]

$$\upsilon_B^{+} = \left(2k_B T_f/m(d_s)/\pi\right)^{\frac{1}{2}}\Big/u_* \tag{8}$$

Note that Eq. 7 serves the boundary condition for the transport equation (Eq. 6).

It is a common practice for deposition characterization, instead of particle size to use the Stokesian particle relaxation time (e.g., Guha[20])

$$\tau_s = \frac{\rho_s d_s^2}{18\mu_f} \tag{9}$$

In a case of small particle relaxation times, the concentration of solids suspended in either a Couette or a pipe flow is uniform except the close wall vicinity. Therefore, instead of the whole pipe cross section we can consider a small computational domain near the wall. To be confident in the modeling results, we will select a relatively large domain with the outer boundary located on the distance $y^{+} = 30$ from the wall.

Then the second boundary condition for the transport equation (Eq. 6) is

$$c^{+}(30) = 1 \tag{10}$$

Fortunately the dimensionless eddy diffusivity within this domain can be calculated by the simple empirical correlations (Lin et al.[21])

$$\begin{aligned} \varepsilon_t^{+} &= \frac{y^{+}}{5} - 0.959 \qquad && 5 < y^{+} \le 30 \\ \varepsilon_t^{+} &= \left(\frac{y^{+}}{14.5}\right)^3 \qquad && y^{+} \le 5 \end{aligned} \tag{11}$$

where $\varepsilon_t^{+} = \varepsilon_t/\nu_f$, ε_t is the eddy diffusivity.

Then Sc_t the turbulent diffusivity is (e.g., Bird[10])

$$D_t^{+} = \frac{\varepsilon_t^{+}}{Sc_t} \tag{12}$$

where Sc_t is the turbulent Schmidt number.

According to the mass- and heat-transfer experimental data, the turbulent Schmidt number is smaller than unity (e.g., Schlichting and Gersten[22]). Because the system considered here is composed of small particles following fluid, we employed $Sc_t = 0.85$ in our calculations (e.g., Schlichting and Gersten[21] recommended $Sc_t = 0.87$ for turbulent heat transfer).

Analytical solution of Eq. 6 with the boundary conditions (Eqs. 7 and 10) is as follows

$$V_{dep}^{+} = \frac{1}{2}\gamma c^{+}\left(r_s^{+}\right)\upsilon_B^{+}$$

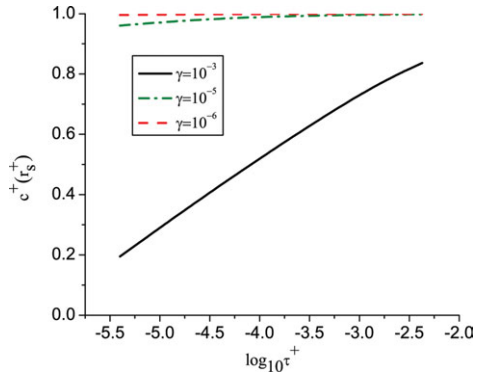

Figure 2. Dimensionless particle concentration at the wall vs. particle relaxation time at different particle-wall sticking probabilities.

where

$$c^+\left(r_s^+\right)=\frac{1}{1+\frac{1}{2}\gamma Sc_t v_B^+\times\left[24.06+14.5\left(\psi(5)-\psi\left(r_s^+\right)\right)\right]}$$
$$\psi(\chi)=\frac{1}{6b^2}\ln\left(\frac{\chi+b}{\chi^2-b\chi+b^2}\right)+\frac{1}{b^2\sqrt{3}}\operatorname{arctg}\left(\frac{2\chi-b}{b\sqrt{3}}\right)$$
$$\chi=\frac{y^+}{14.5},\ b=\left(D_B^+Sc_t\right)^{\frac{1}{3}} \tag{13}$$

Based on Eq. 7 we can write the equation for the mass flux of i-th size fraction particles to the wall as

$$q_i=\rho_s V_{depi}^+ u_*=\frac{1}{2}\gamma m_i N_i c_i^+\left(r_i^+\right)u_* v_B^+\left(r_i^+\right) \tag{14}$$

where $c_i^+(r_i^+)$ is the dimensionless concentration of the i-th size fraction particles at the particle radius distance r_i^+ from the wall that is calculated by Eq. 13.

Because we assumed that the particle–particle collision efficiency α does not depend on the particle size, the particle-wall sticking probability γ should be independent of the particle size as well.

Then the total deposition mass flux to the wall is

$$q_\Sigma=\sum_{i=1}^{i_{cr}}q_i=\frac{1}{2}\gamma\sum_{i=1}^{i_{cr}}m_i N_i c_i^+\left(r_i^+\right)u_* v_B^+\left(r_i^+\right) \tag{15}$$

where i_{cr} is the size fraction corresponding to the critical particle size.

To better understand particle behavior in the vicinity of the wall, we calculated the dimensionless concentration of asphaltene particles at the wall for the different particle sizes at the different particle-wall sticking probabilities. In Figure 2 we showed the distributions of $c^+(r_s^+)$ vs. the dimensionless particle relaxation time $\tau^+=\tau_s u_*^2/\nu_f$ for the different particle-wall sticking efficiencies ($\gamma=10^{-3}$, 10^{-5}, 10^{-6}) in logarithmic coordinates. The smallest value of τ^+ corresponds to the particle size $d_s=3$ nm, the largest to the size $d_s=100$ nm. As mentioned previously, the particle-wall sticking probability for asphaltenes is expected to be close to the particle–particle sticking efficiency that is found to be very small ($\alpha\sim10^{-5}$–10^{-6}). From Figure 2 one can see that the dimensionless asphaltene particle concentration at the wall $c^+(r_s^+)$ for such a low-probability γ is very close to unity that indicates nearly uniform concentration distribution over either a pipe or a Couette device cross section. Thus, for determining the asphaltene deposition flux, the calculation of particle concentration at the wall can be waived. Substituting the constant dimensionless particle concentration at the wall $c_i^+(r_i^+)=1$ into Eq. 15, we obtain the equation for the total asphaltene deposition mass flux in the simpler form

$$q_\Sigma=\frac{1}{2}\gamma u_*\sum_{i=1}^{i_{cr}}m_i N_i v_B^+\left(r_i^+\right) \tag{16}$$

Accounting for the shear removal effect

At a relatively high-shear stress at the wall (high-rotation speed of a Couette device spindle), the shear removal of the deposit layer may significantly reduce the deposition rate. In such a case the actual flux of depositing particles to the wall should be adjusted to take this effect into account.

Due to extreme complexity of the shear removal phenomenon, for its description we employed an approach that is to a great extent empirical and based on the following considerations. Because the asphaltene deposit is a solid material of a high strength, we assume that its removal is carried out as a series of discrete removals of chunks of the material forming microroughness (asperities) on the deposit surface. For the sake of simplicity, we substitute the discrete mechanism of the shear removal with a continuous one. Then it is possible to assume that the shear removal rate is proportional to the deposition flux because the growth rate of the deposit layer and the growth rate of microasperities, respectively, are obviously proportional to the deposition flux. Then, the corrected deposit flux is (Eskin et al.[8])

$$q_a=q_\Sigma\cdot\left[1-\alpha_r\left(\frac{\tau_w}{\tau_{w0}}-1\right)^n\right] \tag{17}$$

where n, α_r are the empirical parameters, τ_{w0} is the pseudo-yield shear stress of the deposit material defining the starting condition of the shear removal.

All the parameters of Eq. 17 are identified from the Couette device experimental data.

The population balance model for the flow-through Couette device

The population balance model for the flow-through system is different from that for the batch system (see Eq. 4). The set of population balance equations for the flow-through system, straightforwardly derived by assuming that the Couette device is an ideal mixer, takes the form (Eskin et al.[8])

$$\frac{dN_1}{dt}=\left(\frac{dN_1}{dt}\right)_{batch}+\frac{Q}{W}(N_{01}-N_1)$$
$$\frac{dN_i}{dt}=\left(\frac{dN_i}{dt}\right)_{batch}-\frac{Q}{W}N_i\qquad i=2...im \tag{18}$$

where $N_{01}=\frac{c_0}{v_1}$ is the initial concentration of the particles of the first fraction by number in a fluid flowing in a Couette device at an abrupt pressure reduction, v_1 is the volume of the first fraction particle, Q is the volume flow-through rate, and W is the Couette device volume.

Table 1. Characteristics of the Oil A

Sample information	
Reservoir temperature (K)	370
Saturation pressure at T_{res} (MPa)	19.0
Mass concentration of precipitated asphaltenes at the pressure drop from p_{AOP} to p_s (wt %)	0.45
Asphaltene onset pressure (MPa)	34.5
Viscosity (Pa.s)	1.2e-3
Density (kg/m^3)	742

Application of the Deposition Model to a Flow in the Couette Device

Identification of the model parameters based on Couette device experimental data

In a case, when the shear removal rate is zero the model parameters are (1) the particle–particle collision efficiency α, (2) the particle-wall sticking probability γ, and (3) the critical particle size d_{cr}.

Note that in order to exclude the shear removal effect a few experiments are required to evaluate the rotation speed corresponding to the shear removal start. The shear stress at the wall in this case corresponds to the deposit material pseudo-yield shear stress. The shear removal model coefficients (α_r and n) are determined from the experiments at the rotations speeds providing the shear removal regimes ($\tau_w > \tau_{w0}$).

The mass of the deposit, accumulated on the outer wall of the Couette device during a given time T, is calculated in the same way for batch and flow-through experiments

$$M_t(T) = \int_0^T q_a(t) 2\pi RL dt \qquad (19)$$

The experimental parameter identification procedure is reduced to finding parameter values that minimize the absolute difference between the measured $M(T)$, and the calculated M_t (T) deposit masses ($|\Delta M(T)| = |M(T) - M_t(T)| =$ min).

As previously mentioned, the batch experiment has limited accuracy because of the small deposit mass. Therefore, the most important information that can only be obtained from the batch experiments is an estimate of the time needed for depleting a fluid of particles, which are able to deposit.

Examples of calculating the asphaltene deposition in a Couette device

A number of calculations of the deposition in a Couette device have been performed.

We would like to mention that Eskin et al.[8] presented the modeling results for the two different oils. To confirm the model consistency and increase credibility of the modeling concept, we present here the simulations results for the oil A. The properties of the oil A are shown in Table 1.

Note that in contrast to the simulations presented by Eskin et al.[8] we used the population balance model at neglecting the agglomerate breakage term. This neglecting caused less than 1.5% reduction in the deposition mass calculated.

The experiments were conducted at the spindle rotation speed, which approximately corresponds to the pseudo-yield stress for a deposit layer, i.e., no-shear removal occurs at this speed yet.

We conducted four batch and four flow-through experiments of different durations. Three flow-through experiments were done at a relatively low flow-through rate, $Q = 3$ cc/min, and one at $Q = 10$ cc/min. The identified model parameters are: the particle–particle sticking efficiency $\alpha = 8 \times 10^{-5}$, the particle-wall sticking probability $\gamma = 3.7 \times 10^{-6}$, and the critical particle size $d_{cr} \approx 100$ nm.

We would like to emphasize that the model parameters identified for the oil A are of the same order of magnitude as those reported by Eskin et al.[8]

In Figure 3 one can see the computed deposit mass vs. time for the batch experiments. The deposit mass vs. time for the flow-through experiments at $Q = 3$cc/min is presented in Figure 4. The experimental data are shown by markers in both figures. It is important to note a reasonably good agreement between the predicted and the measured results. The deviations of the predicted data from those measured do not exceed 15% that is within the range of the measurement error. In Figure 5 we showed the calculated dependence of the asphaltene deposition rate (g/m^2/day) on the flow-through rate (the experimental data are also shown by markers). The deposition rate rapidly increases with increasing the flow-through rate. This is because the higher the flow-through rate, the smaller the mean particle size in a Couette device (the particle residence time is not sufficient for a significant particle-size increase) that leads to the higher deposition rate, respectively.

We would like to also note that because both the particle agglomeration and the deposition are governed by the

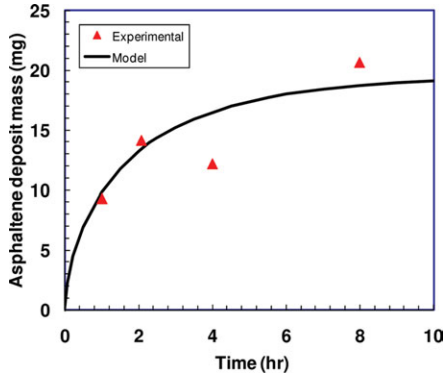

Figure 3. Asphaltene deposit mass on the Couette device wall vs. time in a batch regime.

[Color figure can be viewed in the online issue, which is available at wileyonlinelibrary.com.]

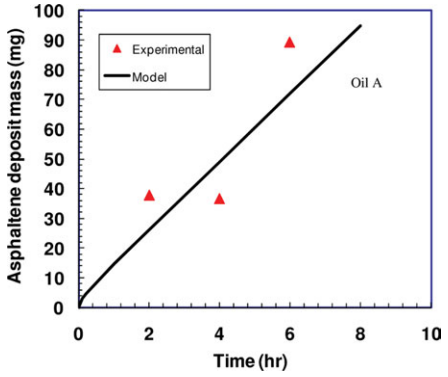

Figure 4. Asphaltene deposit mass on the Couette device wall vs. time in a flow-through regime.

[Color figure can be viewed in the online issue, which is available at wileyonlinelibrary.com.]

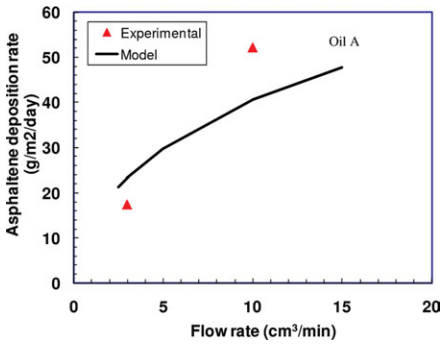

Figure 5. Asphaltene deposition rate vs. flow-through rate.

[Color figure can be viewed in the online issue, which is available at wileyonlinelibrary.com.]

Brownian motion, the Taylor vortices that significantly affect the flow field in a Couette device at Re_c <13,000 should not significantly influence the agglomeration and the deposition at lower Reynolds numbers. Note that this statement is expected to be valid for a developed turbulent flow only because our model requires a uniform particle concentration over a flow domain that is achieved by turbulent mixing. The Wendt correlation for the torque vs. the rotation speed (see Lathrop et al.[12]) can be used for calculating the rotation speed needed for Couette device experiments at Re_c <13,000.

Explanation of the Deposition Characteristics Obtained by the Developed Model on the Basis of Analysis of Asphaltene Particle Interactions

The major characteristics of the asphaltene deposition process that we identified by modeling are the very small size of depositing particles and the extremely low-sticking efficiency. These results were not expected and their plausible explanation is a key step to prove validity of the deposition mechanism accepted as the basis for our model.

The asphaltenes in crude oil have for many years been approached as spherical aggregates composed of a small number of molecules. The exact nature of these agglomerates is still not resolved, but it is known that aggregation persists down to a very low concentration at the ppm level (Merino-Garcia and Andersen[23]). The known experimental studies are mostly conducted with solutions of asphaltenes, not with asphaltenes in natural crude oils. We need to also distinguish between what one may call primary particles stable in oil, and agglomerates which are formed when the solvent conditions of the surrounding liquid media are changed leading to flocculation. The latter is equivalent to a state beyond the flocculation onset threshold (depressurization below AOP pressure in a production tubing), indicating massive precipitation. Hence, in the same system we may have primary particles in equilibrium with larger flocks (agglomerates).

Thus, the deposition on the pipe wall may occur due to adherence of either unstable primary particles or the flocks. It is tempting to assume the primary particles to be partially stable with no driving force causing adherence to the wall surface, and explain that the deposition is caused only by the larger flocks. However, our knowledge from water in oil emulsion stability studies indicates that the stability is highest as we approach the onset, and decrease as solid flocks are formed (see Figure 6 based on Juhl's data[24]). Here the oil/water interface is taken as an analog to the oil/pipe wall interface. It is known from emulsion studies that just below the flocculation onset, where agglomeration is not yet taking place to a significant extent, the particles are more prone adhering to the interface than in well dispersed asphaltene-toluene solutions. Beyond the flocculation onset one can observe a rapid decrease in the asphaltene emulsion stability.

In accordance with the assumed analogy one may expect that the asphaltene behavior at the solid/liquid (the wall surface) interface is similar to that at the liquid/liquid (emulsion) interface. Because the major driving force of asphaltene transport to the solid surface is the Brownian motion that does not depend on a flow pattern, it is clear that the mechanism of particle transport to the oil/water interface has to be the same. Thus, agglomerates are less prone to deposit on the liquid/liquid interface and the solid surface, respectively than primary particles. Thus, the discussed analogy is a plausible justification of the critical particle-size concept imposing the restriction on the maximum size of a particle that is able to deposit.

The adherence of the asphaltene particles to the initially asphaltene/oil coated surface is assumed to be related to the particle–particle interaction. Asphaltene structuring in literature is most often assumed to occur through stacking aromatic sheets and stack growth inhibition by steric hindrance. Assuming asphaltenes are surrounded by coronas of alkyl chains as suggested by Carbognani and Rogel[25] one would expect repulsion between them. Andersen[26] recently suggested that the particle growth limitation, and the particle–particle repulsion are phenomena necessary to explain behavior of some properties of asphaltene solutions. Those ideas were based on experiments with solutions at the asphaltene concentration from 0.1 to about 5 g/L. Roux et al.[27] also showed using small angle neutron scattering (SANS) that asphaltene particle size increases up to about 5 nm at a certain concentration and then shrinks slightly (by 20–30%) as the concentration increases. Data from Roux et al.[27] are plotted in Figure 7. This observation could lead to a guess that asphaltene particles are repulsive with very little adherence. However, in average an asphaltene molecule has only 50 wt % of carbon in aromatic structures and about 5–10 wt % of nitrogen, sulfur or oxygen containing functional groups. The question is how the corona of alkyl chains can interact strongly with the layers of asphaltenes covering the pipe wall leading to actual adherence and deposit layer buildup.

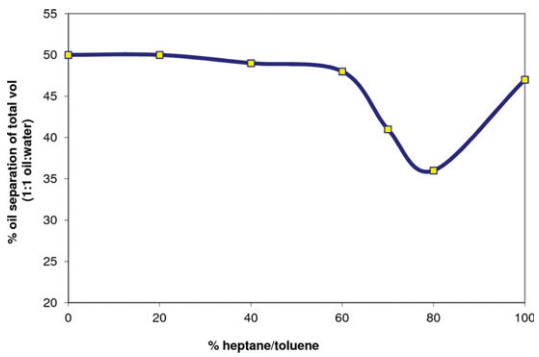

Figure 6. Effect of oil composition (heptanes/toluene) on oil-phase separation from a water in oil model emulsion for 10 h; the asphaltene concentration is 1 g/L (data from Juhl[24], 1999).

[Color figure can be viewed in the online issue, which is available at wileyonlinelibrary.com.]

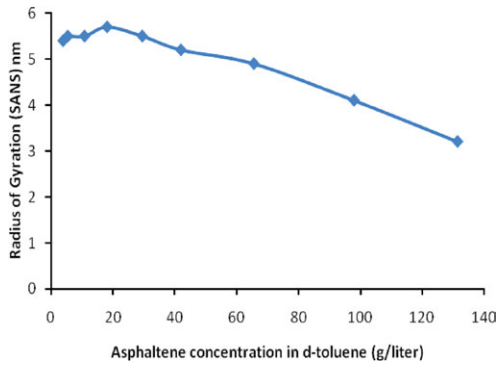

Figure 7. Asphaltene particle size by SANS vs. concentration in d-toluene at 40°C (data from Roux et al.[27])

[Color figure can be viewed in the online issue, which is available at wileyonlinelibrary.com.]

If the analogy with the water-oil interface reflects the way asphaltene particles interact with each other, one could expect that the alkyl corona type of molecules do not have any significant attraction to the interface, while the particles carrying functional groups (COOH, NH, OH, SH, etc.) may adhere to the interface. The number of these functional groups is obviously limited, and, therefore, a particle–particle sticking requires a certain mutual orientation of the functional groups belonging to individual interacting particles. After adherence occurred, further entanglement of the corona alkyl chains could increase the strength of the interaction, and finally a reorientation of particles composing the agglomerate might take place during a ripening process. This hypothesis about the mechanism of asphaltene interactions allows us to explain both observations:

1. Asphaltene particle sticking probability is very low.
2. Only very small particles participate in deposition.

The cause of the first observation has already been clarified. The physics of the second observation can be explained as follows. The primary bonding between particles, caused by the mentioned functional groups is very weak, therefore, only nanoparticles, possessing very low inertia, may stick to each other. A further increase in the agglomerate strength caused by corona alkyl chain entanglement explains an existence of relatively large stable agglomerates of asphaltene particles in a solution, and also a high strength of the asphaltene deposit layer formed on the pipe wall.

Computation of the Asphaltene Deposition in a Pipeline

The model

The population balance approach is applied to a pipeline in terms of the pipe length. Let us consider the pipe flow system as follows. A cylindrical flow element, the cross section of which equals the pipe cross section and the length is dx, moves along a pipe with the mean flow velocity $U(x)$. Particles precipitate due to the pressure drop caused by the viscous friction and the hydrostatic effect. The latter contribution in the pressure gradient has to be taken into account in vertical pipes only. The set of population balance equations for a pipe flow is written as (Eskin et al.[8])

$$\frac{dN_1}{dx} = \frac{1}{U(x)}\left(\frac{dN_1}{dt}\right)_{batch} + \left(\frac{dN_1}{dp}\right)_{pr}\frac{dp}{dx}$$
$$\frac{dN_i}{dx} = \frac{1}{U(x)}\left(\frac{dN_i}{dt}\right)_{batch} \qquad i = 2...im \tag{20}$$

where $dx = U(x)dt$ is the increment of the axial coordinate, and is the particle precipitation rate (the rate of generation of particles of the first-size fraction with the pressure decrease), that can be determined by the precipitation model.

A small increment of the deposit layer thickness during time dt is calculated by considering the mass balance for a small layer element as (Eskin et al.[8])

$$d\delta(x,t) = \frac{q_a(x,t)dt}{\rho_s(1-\varphi)} \tag{21}$$

φ deposit layer porosity that can be determined by the experimental deposit analysis.

Note that in the earlier article Eskin et al.[8] employed this equation for calculation of the final deposit layer profile. The authors[8] assumed that the total deposit layer thickness can be straightforwardly evaluated if instead of increment dt substitute into Eq. 21 the total operation time T_0; i.e., the thin layer approximation was extended to a thick-layer case. However, this assumption looks too strong if an accurate deposition analysis is needed. A growing deposit layer causes a variation of the mean flow velocity along a pipe that leads to nonuniform distributions of both the shear stress and the residence time of transported asphaltene particles. These nonuniform distributions cause variations of the shear removal effect and the deposition flux along a pipe over time. Accounting for these phenomena is important for accurate deposition modeling.

Note also that in their work Eskin et al.[8] for the sake of simplicity neglected a reservoir effect on a flow rate reduction caused by tubing obstruction with the deposit.

Furthermore, we present an improved simulation technique, which is free of several strong assumptions accepted for the simplified model of Eskin at al.[8]

A method of simulation of an asphaltene layer deposit growth in a vertical tubing during production from a simple cylindrical reservoir

Let us consider the precipitation rate term $PR = \left(\frac{dN_1}{dp}\right)_{pr}\frac{dp}{dx}$. Although the total pressure gradient in a vertical pipe $\frac{dp}{dx}$ is determined as a superposition of the frictional gradient and the hydrostatic gradient ($-\rho_f g$), the frictional gradient contribution is relatively small. This is why the asphaltene deposition is significantly more serious problem for vertical pipelines than for horizontal ones, where the hydrostatic pressure gradient is zero. Thus, for engineering calculations of the asphaltene deposition, the total pressure drop in a vertical pipe can be assumed to be equal to the hydrostatic pressure drop. The term $\left(\frac{dN_1}{dp}\right)_{pr}$ is a function of a fluid composition and can be determined by either the asphaltene precipitation model or evaluated on the basis of experimentally measured concentration of precipitated asphaltene particles in a hydrocarbon fluid at pressure reduction from the asphaltene onset precipitation pressure (p_{AOP}), to the bubble point pressure (p_b). Any precipitation model can be used within the modeling approach developed. Analysis of the

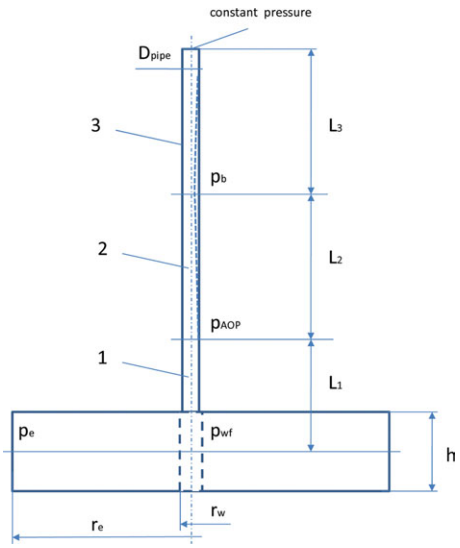

Figure 8. Diagram of the production system considered.

[Color figure can be viewed in the online issue, which is available at wileyonlinelibrary.com.]

precipitation model of Du and Zhang[17] showed that an assumption is a reasonable approximation for engineering calculations. Thus, we may assume that the precipitation rate PR in a vertical pipeline is constant.

As the deposit layer grows, the production rate decreases and in its turn affects the deposit growth rate. On the one hand, the production rate depends on both the bottom-hole pressure, i.e., the pressure in the wellbore at the reservoir level, and the total frictional pressure loss in a pipe. The latter is a function of both the deposit layer profile and the production rate. The bottom-hole pressure is a function of the production rate and the reservoir pressure. This function (the reservoir characteristic) is unique for each reservoir and, in practice, evaluated by a well test. Thus, the deposit layer growth in a production tubing is a complicated phenomenon that depends on the reservoir characteristic and mutually depends on the production rate.

To illustrate the asphaltene deposition in a system composed of wellbore and vertical tubing, we made a few simplifications. Let us consider a cylindrical reservoir (see Figure 8) of the radius r_e and the height h; the wellbore radius is r_w; the rock permeability equals k; the reservoir pressure is p_e. For the steady-state regime with the production rate Q, the pressure drop across the reservoir is (e.g., Dake [28])

$$p_e - p_{wf} = \frac{Q\mu_f}{kh}\left(\ln\left(\frac{r_e}{r_w}\right) + s\right) \tag{22}$$

where p_{wf} is the bottom-hole pressure, and s is the skin factor.

Note that in this work, we assume the constant reservoir pressure p_e during the well operation time T_o (this condition takes place when water flood (e.g., Dake[28]) is employed).

Let us consider the tubing composed of the three sections (Figure 8) denoted as 1, 2 and 3. We will determine the lengths of these sections as follows. The length of the 1st section corresponds to the height of the hydrostatic column, along which the pressure drops from the bottom-hole pressure p_{wf} to the asphaltene onset precipitation pressure p_{AOP}; i.e., we consider only cases, where $p_{AOP} < p_{wf}$. The length of the 2nd section is equal to the height of the hydrostatic column, corresponding to the difference between the onset precipitation pressure p_{AOP}, and the bubble-point pressure p_b. It is expected[1] that the deposit thickness reaches maximum approximately at a tubing cross section corresponding to p_b. For the sake of simplicity we will assume that the length of the 3rd tubing section equals to the length of the 2nd section. This assumption is not significant because the length of the 3rd section is not needed for our calculations (see "Computational Examples and Discussion"). The 3rd section is characterized by a multiphase flow regime. A flow pattern in this section depends on a fluid composition and may change along the tubing due to both pressure reduction and variation of the tubing cross-sectional area caused by a partial obstruction with the deposit. Therefore, both the frictional pressure loss and the hydrostatic pressure drop along this section can hardly be modeled accurately.

As the deposit layer is formed, the flow rate decreases that leads to an increase in the bottom-hole pressure (see Eq. 22) and a downward displacement of the positions of the tubing cross sections corresponding to the p_{AOP} and p_b pressures, respectively. Let us limit our simplified analysis to reservoirs with relatively high permeabilities ($\sim$0.3 Darcy (1 Darcy$\approx 10^{-12}$ m^2) and higher). Then, the mentioned bottom-hole pressure increase, in terms of the hydrostatic column height, is small and can be neglected. Therefore, we will assume that a position of the incipient deposition cross section (characterized by p_{AOP}) is unchangeable.

To calculate variation of the production rate over time, we need to determine evolution of the total pressure loss across the system analyzed. However, because this loss and the production rate are mutually dependent, an additional condition for calculation of the flow system is needed. For the illustration purpose only, let us assume that the total frictional pressure drop, composed of the pressure drop across the reservoir and the pressure drop along the three considered tubing sections, is constant. This condition means that the upper end of the tubing is located on an imaginary surface, where the pressure is constant.

The pressure drop across the reservoir is calculated by Eq. 22. The frictional pressure drop along the 1st and the 2nd tubing sections can be calculated as the pressure drop for a turbulent flow in a circular channel (e.g., by Eq. 1). The cross section of the 2nd tubing section, varying over time, is calculated from the deposition modeling data. To avoid computation of a multiphase flow through the 3rd tubing section, which is beyond the scope of this work, we assume that the pressure drop along this section is equal to that through the 2nd section. This assumption is also made for the illustration purpose only.

The algorithm of calculation of the described simplified production system, operating under conditions of asphaltene deposit growth, consists of the four stages, which have to be repeated at each computational time step dt

1. The particle-size distribution is calculated by the population balance submodel.
2. The theoretical and then the actual deposition fluxes are determined.
3. The deposit layer increment during the time dt is calculated and the tubing radius distribution is updated.
4. The flow rate is updated based on the condition formulated: the pressure drop along the considered production system is constant.

Although the described flow system is simplified, its behavior is expected to be qualitatively similar to behavior of a real production well. A calculation example follows below.

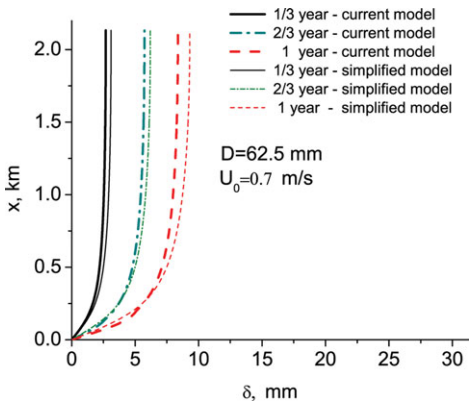

Figure 9. Asphaltene deposit layer thickness distribution along a vertical production tubing at different production times.

[Color figure can be viewed in the online issue, which is available at wileyonlinelibrary.com.]

Computational Examples and Discussion

We conducted numerical studies of asphaltene deposition in a vertical production tubing.

Comparison of the model developed with the simplified model[8]

At the first stage of these studies, we performed deposition calculations for the same oil A (see section "Examples of calculating the asphaltene deposition in a Couette device") transported from the cylindrical reservoir through the production tubing of a relatively small diameter ($D = 62.5$ mm) during a period of 1 year. The reservoir sizes were: the outer radius $r_e = 500$ m; the height $h = 30$ m; the wellbore radius $r_w = 0.089$ m. The rock permeability was k = 0.3 Darcy. The reservoir pressure was constant and equal to $p_e = 41.4$ MPa. The length of the first tubing section was $L_1 = 847$ m, and the 2nd section $L_2 = 2133$ m. The length of the 3rd section was not needed for the accepted problem formulation. As we mentioned previously, the pressure drop along that section was roughly assumed to be equal to that along the growing deposit section. The coefficients of the shear removal model were evaluated by the Couette device experiments at different rotation speeds. The pseudo-yield stress at the Couette device wall was $\tau_{w0} = 0.94$ Pa that corresponds to the mean flow velocity $U = 0.64$ m/s. The other coefficients of the shear removal term (Eq. 17) were $\alpha_r = 0.45$ and $n = 0.30$.

In Figures 9 and 10 we compared the calculation results, obtained by the algorithm described earlier, with the data calculated by the earlier (simplified) model.[8] The graphs obtained by the simplified model are shown by the thin lines. The only growing portions of deposit layer profiles are shown. In Figure 9 one can see the deposit profiles at the different operation times ($T_0 = 1/3$ year, $2/3$ year and 1 year) for the initial mean flow velocity $U = 0.7$ m/s. The deposit layer thickness is almost linearly proportional to the operation time. The deposit layers calculated by the model developed are thinner than those obtained by the simplified model. In Figure 10 we showed the deposit layer thickness distributions along the same tubing for the different initial mean flow velocities: $U = 0.7$, 1.3, 2.0 m/s. The maximum layer thickness (~30% of the tubing radius) was observed at the lowest mean flow velocity used for this example.

The major reason of some discrepancy between the results obtained by the two models is obvious. The mean flow velocity is nonuniformly distributed along a pipe, partially obstructed with the deposit. The velocity increases along a pipe because the flow cross section decreases due to increasing the deposit layer thickness. The higher the velocity is, the stronger the shear-removal effect causing a deceleration of the layer thickness growth (see Figures 9 and 10). The simplified model employs the constant flow velocity that is equal to that through the unobstructed pipe cross section. That velocity is lower than the velocity level in the tubing section, significantly obstructed with the deposit. Another cause of the differences in the deposit layer profiles, calculated by the developed and the simplified models, is the different particle residence-time distributions along a tube that control the deposition flux distributions. The higher the flow velocity is, the shorter the particle residence time that causes a reduction of the particle-size level due to agglomeration, and, therefore, leads to the corresponding increase in the deposition flux. However, from Figures 9 and 10 one can conclude that in our study case, the deposition flux variation along tubing caused by the nonuniform particle residence-time distribution has a less pronounced effect on the deposit thickness than the shear removal.

Thus, the deposition model developed provides thinner deposit layer than the simplified model, published earlier.[8] Nevertheless, the differences in the results are moderate. Taking into account uncertainties, associated with reservoir properties, and difficulties of accurate calculation of pressure losses in a pipe section operating in a multiphase flow regime, we can conclude that a practical application of the simplified model is justified for engineering estimations.

Qualitative comparison of the modeling results with the field observations[1]

Although, our computations demonstrated self-consistency of the modeling approach developed, we would like to note that the deposit layer profiles, measured by Haskett and Tartera[1] in the field, are noticeably different from those obtained by our model. Obviously, those disagreements are caused by the bottom-hole pressure reduction in the field cases studied by Haskett and Tartera.[1] Due to reservoir depletion, the bottom-hole pressure was significantly decreasing in those

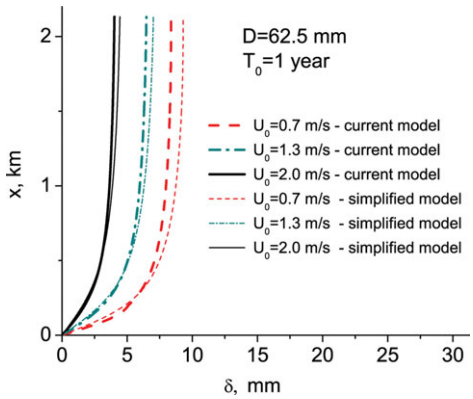

Figure 10. Asphaltene deposit layer thickness distribution along a vertical production tubing at different initial mean flow velocities.

[Color figure can be viewed in the online issue, which is available at wileyonlinelibrary.com.]

cases, while our calculations, illustrated by Figures 9 and 10 were performed at the constant bottom-hole pressure.

Let us demonstrate that an introduction of the bottom-hole pressure reduction into the deposition model allows obtaining the deposit layer profiles, which are in a qualitative agreement with the field observations.[1] Reservoir depletion is a complex process that depends on reservoir parameters and production tubing geometry. To simplify our analysis, we assume that a depletion scenario is given. Then, due to reservoir depletion, the bottom-hole pressure p_{wf}, decreases by Δp_t during the operation time T_o. A decrease in p_{wf} leads to displacement of both the tubing cross sections corresponding to the onset precipitation pressure, and the bubble-point pressure down the well. This displacement is equal to the hydrostatic column height, corresponding to the given bottom-hole pressure decrease.

The total length of the tubing section obstructed with the deposit is

$$L_{dep} = \frac{p_{AOP} - p_b + \Delta p_t}{\rho_f g} \tag{23}$$

Then the x-coordinate changes within this section in the following range $x \in \left[-\frac{\Delta p_t}{\rho_f g}, \frac{p_{AOP}-p_b}{\rho_f g}\right]$

The profile of the deposit layer, formed along the defined tubing section during the operation time T_o, is calculated as follows

$$\delta(x, dt) = \frac{1}{\rho_s(1-\varphi)} \int_0^{T_o} q_a\left(x + \frac{\Delta p(t)}{\rho_f g}, t\right) dt \tag{24}$$

$$\text{For } x \in \left[-\frac{\Delta p(t)}{\rho_f g}, \frac{p_{AOP} - p_b - \Delta p(t)}{\rho_f g}\right]$$

q_a is calculated by Eqs. 16 and 17

$$\text{For } x \in \left]\frac{p_{AOP} - p_b - \Delta p(t)}{\rho_f g}, \frac{p_{AOP} - p_b}{\rho_f g}\right]$$

$$\text{and } x \in \left[-\frac{\Delta p_t}{\rho_f g}, -\frac{\Delta p(t)}{\rho_f g}\right[$$

$$q_a = 0$$

where $\Delta p(t)$ is a function describing the reduction of the bottom-hole pressure during the time t.

We illustrated a deposition model performance in a depleting reservoir by using the same oil A, employed in the previous numerical examples. For illustration purpose only, we assumed that due to reservoir depletion, the bottom-hole pressure linearly decreases by $\Delta p_t = 1000$ psi during the operation time $T_o = 1$ year. The initial mean flow velocity was $U_0 = 0.7$ m/s. Because the calculations presented before, demonstrated that the simplified model[8] shows a reasonably good performance compared with the developed (improved) model, we employed the simplified model for these computations. Since the characteristics of a real production system, composed of reservoir and tubing are unknown, following the simplified approach,[8] we calculated the deposition process by using the constant flow velocity $U = U_0$.

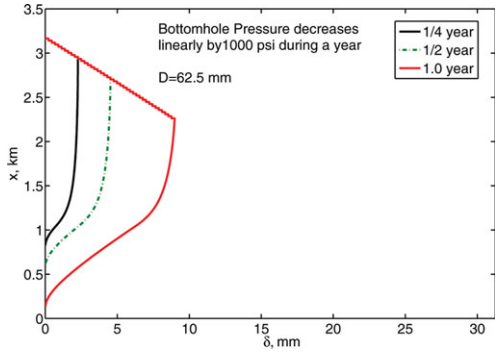

Figure 11. Asphaltene deposit layer thickness distribution along a vertical production tubing at different production times (the depleting reservoir case).

[Color figure can be viewed in the online issue, which is available at wileyonlinelibrary.com.]

In Figure 11 one can see the deposit layer profiles, computed for the different operation times $T_o = 1/4$, $1/2$, and 1.0 year. A qualitative agreement of the modeled deposit profiles with those, reported by Haskett and Tartera[1] is obvious. Note that the comparison is justified only for the tubing region, where the pressure exceeds the bubble point during the entire operation time. As this was mentioned previously, our model assumes that both the precipitation and the deposition processes stop as soon as the pressure drops below p_b.

The result obtained (Figure 11) is the strong confirmation of validity of our deposition model. We obtained the deposit layer profiles, which are qualitatively similar to those observed in the field, without using any additional fitting parameters. Thus, an incorporation of the deposition model developed into a software for calculation of the oil production system (reservoir + tubing), will allow reliable prediction of the asphaltene deposition under field conditions.

Conclusions

Asphaltene deposition phenomena have been investigated both theoretically and experimentally. A Couette device, where the inner cylinder rotates and particles deposit on the outer wall, has been used for deposition laboratory studies. The deposition modeling approach, recently proposed by the authors (Eskin et al.[8]) has been improved. The deposition model is composed of the submodels describing asphaltene agglomerate growth and their transport to the wall. The agglomerate growth model has been simplified without reducing its accuracy and the more accurate model of particle transport to the wall has been developed. According to the deposition model, tuned by the experimental data, only submicron asphaltene particles can deposit on the pipe wall and only a very small fraction of particles touching the wall sticks to the surface. Those phenomena have been explained based on an analogy between the deposition and water in oil emulsion stabilization by asphaltenes, and on an analysis of interaction of asphaltene molecules. The deposition model performance has been illustrated by modeling of oil production, accompanied with asphaltene deposition, from a cylindrical reservoir through vertical tubing. The computations, performed for a reservoir depleting over time, demonstrated a good qualitative agreement with the filed data reported in literature.[1]

Literature Cited

1. Haskett CE and Tartera M. A practical solution of the problem to the asphaltene deposits-Hassi Messaoud field, Algeria. *J Petrol Technol*. 1965;387–391.
2. Alkafeef SF, Al-Medhadi F, Al-Shammari AD. A simplified method to predict and prevent asphaltene deposition in oilwell tubings: field case. *SPE Production & Facilities*. 2005:126–132.
3. Ramirez-Jaramillo E, Lira-Galeana C, Manero O. Modeling asphaltene deposition in production pipelines. *Energy Fuels*. 2006;20: 1184–1196.
4. Burger E, Perkins T, Striegler J. Studies of wax deposition in the Trans Alaska pipeline. *J Petrol Technol*. 1981;33:1075–1086.
5. Akbarzadeh K, Ratulowski J, Lindvig T, Davis T, Huo Z, Broze G. The importance of asphaltene deposition measurements in the design and operation of subsea pipelines. SPE paper. 2009; #124956.
6. Soulgani BS, Rashtchian D, Tohidi B, Jamialahmadi M. Integrated modeling method for asphaltene deposition in wellstring. *J Jap Petrol Inst*. 2009;52:322–331.
7. Vargas FM, Creek JL, Chapman WG. On the development of an asphaltene deposition simulator. *Energy Fuels*. 2010;24:2294–2299.
8. Eskin D, Ratulowski J, Akbarzadeh K, Pan S. Modeling asphaltene deposition in turbulent pipeline flows. *Can J Chem Eng*. 2011;89: 421–441.
9. Rahmani NHG, Dabros T, Masliyah JH. Evolution of asphaltene floc size distribution in organic solvents under shear. *Chem Eng Sci*. 2004;59:685–697.
10. Bird RB, Steward WE, Lightfoot EN. *Transport Phenomena*. New York, NY: John Wiley & Sons; 2002.
11. Eskin D. An engineering model of a developed turbulent flow in a Couette device. *Chem Eng Process*. 2010;49:219–224.
12. Lathrop DP, Fineberg J, Swinney HL. Transition to shear-driven turbulence in Couette-Taylor flow. *Phys Rev A*. 1992;46:6390–6405.
13. Fotland P, Askvik KM. Determination of Hamaker constants for asphaltenes in a mixture of pentane and benzene. *Colloids Surf A*. 2008;324, 22–27.
14. Flesch JC, Spicer PT, Pratsinis SE. Laminar and turbulent shear-induced flocculation of fractal aggregates. *AIChE J*. 1999;45:1114–1124.
15. Rastegari K, Svrcek WY, Yarrnaton HW. Kinetics of asphaltene flocculation. *Ind Eng Chem Res*. 2004;43:6861–6870.
16. Levich VG. *Physicochemical Hydrodynamics*. Engelwood Cliffs, NJ: Prentice-Hall; 1962.
17. Du JL, Zhang D. A thermodynamic model for the prediction of asphaltene precipitation. *Petrol Sci Technol*. 2004;22:1023–1033.
18. Betancourt SS, Ventura GT, Pomerantz AE, Viloria O, Dubost FX, Zuo J, Monson G, Bustamante D, Purcell JM, Nelson RK, Rodgers RP, Reddy CM, Marshall AG, Mullins OC. Nanoaggregates of asphaltenes in a reservoir crude oil and reservoir connectivity. *Energy Fuels*. 2009;23:1178–1188.
19. Maqbool T, Raha S, Hoepfner M.P, Fogler HS. Modeling the aggregation of asphaltene nanoaggregates in crude oil-precipitant systems. *Energy Fuels*. 2011;25:1585–1596.
20. Guha A. Transport and deposition of particles in turbulent and laminar flow. *Annu Rev Fluid Mech*. 2008;40:311–341.
21. Lin CS, Moulton RW, Putnam GL. Mass transfer between solid wall and fluid streams: Mechanism and eddy distribution in turbulent flow. *Ind Eng Chem*. 1953;45:636–640.
22. Schlichting H, Gersten K. *Boundary-Layer Theory*. Berlin, Heidelberg, New York: Springer-Verlag; 2000.
23. Merino-Garcia D, Andersen SI. Calorimetric evidence about the application of the concept of CMC to asphaltene self-association. *J Dispersion Sci Tech*. 2005;26:217–225.
24. Juhl LU. Water-in-Crude Oil Emulsion Stability (in Danish) [MSc Thesis]. Dept. Chem. Eng. Technical University of Denmark; 1999.
25. Carbognani L, Rogel E. Solvent swelling of petroleum asphaltenes. *Energy Fuels*. 2002;16:1348–1358.
26. Andersen SI. In: Birdi KS, ed. *Handbook of Surface and Colloid Chemistry*. 3rd ed. CRC Press; 2009.
27. Roux J-N, Broseta D, Deme B. SANS study of asphaltene aggregation: Concentration and solvent quality effects. *Langmuir*. 2001;17:5085–5092.
28. Dake LP. *Fundamentals of Reservoir Engineering*. New York: Elsevier; 1978.

Manuscript received Jun. 6, 2011, and revision received Oct. 7, 2011.